Monolithic 300 Gb/s parallel transmitter in InP based generic photonic integration technology

Monolithic 300 Gb/s Parallel Transmitter in InP based Generic Photonic Integration Technology

Weiming Yao, *Member, IEEE,* Meint K. Smit, *Fellow, IEEE,* and Michael J. Wale, *Member, IEEE*

***Abstract*—In order to meet the constantly rising traffic demands in optical transport systems for data and telecommunications, compact, power efficient and low cost optical transmitters are needed that offer easy scalability towards higher transmission capacities. Photonic integrated circuit (PIC) technology based on the InP material has long enabled the monolithic integration of tunable sources with modulators and opened the way towards large-scale wavelength-division multiplexed (WDM) parallel transmitters. In this paper, we present the design and performance of a monolithic tunable 8×40 Gb/s parallel transmitter chip with more than 220 components and state-of-the-art capacity density metric. A generic photonic integration approach was followed, in which the transmitter is constituted from well-developed subcircuits and building blocks (BB), facilitating its design and manufacturing. With the trend towards large-scale integration with increasing component densities and smaller chip sizes, proximity effects in form of crosstalk are limiting further miniaturization efforts. We analyze electrical, thermal and optical crosstalk effects that are relevant to the transmitter design, discuss appropriate mitigation techniques and indicate the limitations of the current technology.**

***Index Terms*—Photonic integrated circuits, optoelectronics, tunable transmitter, WDM transmitter**

I. Introduction

PHOTONIC integrated circuit (PIC) technology has revolutionized the optical component industry since the advent of the first optoelectronic integrated devices in the 1980s. Various integration concepts ranging from hybrid, heterogeneous up to monolithic integration have been followed in both research and industry, each with their advantages and drawbacks. The latter approach has gained recent popularity and proves to be successful as PICs move towards higher complexity and component numbers, driven by telecom and datacom applications that require increased functionality and capacity at lower cost and power consumption. The ability to integrate a multitude of optical components monolithically on the same semiconductor substrate and form complex chips is integral to meet those requirements. Here, InP-based PICs can combine efficient active devices with low-loss passive components and therefore save on optical coupling losses, chip space and assembly costs with respect to other material systems such as silicon. This advantage is reflected in the wide adoption of InP devices in commercial products for the optical transceiver industry [1]. For an integration technology to be truly successful it has to be scalable towards higher volumes and it is clearly advantageous for it to be accessible at a low cost. The generic integration approach to photonic circuit design and manufacturing offers a significant reduction in prototyping costs [2]. Application specific circuits such as high-capacity optical transmitters are then constructed from well-developed sub-circuits or building blocks which are in turn based on an underlying generic integration platform technology. This approach has resulted in the successful fabrication of several multi-channel optical transmitters [3], [4], facilitating the entire production cycle from circuit design up to device fabrication and contributing to the continued success of monolithic photonic integration on InP.

Next to the emergence of generic integration platforms, we can observe a shift towards small form-factor pluggable optics [5], Tb/s transmitter capacities [6] and a need to further reduce cost and power consumption [7], so that optical transmitters have gained in total complexity and integration density and evolved to large-scale PICs [8]. In fact, the InP chip complexity has increased exponentially with time, displaying a doubling of the component count per chip every 3 years, which is often named as the equivalence of Moore's law in photonics [9]. At the same time, steady efforts in size reduction of photonic circuits drive chips to ever increasing component densities. This causes undesired proximity effects between components in form of electrical, thermal and optical crosstalk to arise, resulting in performance degradations which pose a limit to further miniaturization and capacity increase [10]–[12]. A thorough understanding of these effects and their possible mitigation is therefore essential in order to sustain the rapid development of high-capacity optical transmitters and the continued success of integrated photonics technology.

In this paper we present the detailed design and characterization results of an 8-channel parallel transmitter fabricated in an experimental generic integration platform as an example of a high density PIC and to illustrate the capabilities and limitations of such approaches. Initial results of the device have been reported in [13]. In contrast to custom integration where the integration process can be optimized to yield best performance for the given device, generic integration platforms focus on a variety of basic building blocks, from which more advanced circuits can be constructed. In addition, the process technology has to be kept as simple as possible and at the same time guarantee the proper functioning of all building blocks. This limits inevitably the complexity of the process and epitaxial design choices, leading in particular cases to compromises in device performance compared to custom integration processes. Nevertheless, we show that the transmitter is comparable to state-of-the-art demonstrators from the literature and exhibits to the best knowledge of the authors the highest aggregate capacity and density within generic integration platforms so far. We paid special attention to performance impairments due to proximity effects that result in crosstalk during its design. We first discuss the chip architecture in section II and elaborate

on the intensity modulation direct detection (IM/DD) parallel transmitter scheme we utilized for this work. In section III, proximity effects that are relevant to this demonstrator design are discussed in detail, in particular RF crosstalk between transmission lines and modulator electrodes, thermal crosstalk between laser arrays and optical back reflections and their influence on the laser behavior. Appropriate design guidelines and measures are indicated which can lead to crosstalk reduction. The performance of the fabricated transmitter chip is reported in section IV and a short discussion on further scalability and future prospects are given. Finally, we summarize the paper in section V.

II. Parallel Transmitter Architecture

The idea of parallelism has existed in optical transmission systems since the introduction of wavelength-division multiplexing (WDM) and was adopted in early monolithically integrated multi-channel transmitters [14] since photonic integration can readily provide for a large number of parallel channels. However, with the emergence of coherent optical communications in combination with the capabilities of digital signal processing [15], the transmission capacity could be increased by means of higher spectral efficiencies per wavelength, using advanced modulation formats [16]. As a result, transmitter PIC development focused on vector modulation in combination with polarization-diversity schemes in order to yield record high bit rates per wavelength so far [17]–[19]. This direction, however, starts to be constraint by upper bounds in capacity, imposed through fundamental signal-to-noise limitations in transmission channels [20]. At the same time, the analog bandwidth of transmitters only increased slowly over time due to technical challenges in high-speed modulator development and high-speed electronics [21], [22]. Consequently, to further increase in capacity, parallelism has to be included and exploited again more extensively in transmitter designs beyond a few channels and is believed by many to be a necessary next step [23]. Initial efforts implement this concept even into the spatial domain by utilizing multi-core and multi-mode multiplexing, emphasizing the need for parallelism [24]. It is therefore only a matter of time, before scaling towards higher channel counts in monolithically integrated transmitters become urgent again. Prominent examples in recent literature based on highly specialized integration platforms can be found in [6], [25].

In this work, we utilize an experimental generic integration platform based on InP substrate to realize an 8-channel IM/DD transmitter. The platform allows for the co-integration of highly efficient DBR lasers with high-speed capacitively-loaded traveling-wave Mach-Zehnder modulators (TW-MZM) and was developed with support from the European PARADIGM research project [26]. IM/DD schemes can reduce overall system complexity, cost and power consumption, at the expense of shorter transmission reach, lower spectral efficiency and a lack of transmission impairment compensation. Yet, for short-reach applications such as access networks and data center communications it poses a viable solution to cope with stringent cost and power requirements [27].

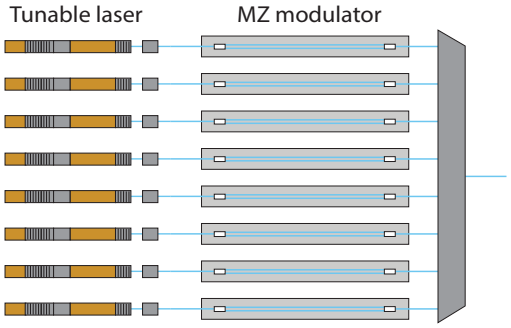

Fig. 1: Illustration of parallel transmitter architecture which permits easy scaling towards higher bitrates through the utilization of many λ channels and can easily be realized through monolithic large-scale integration of components.

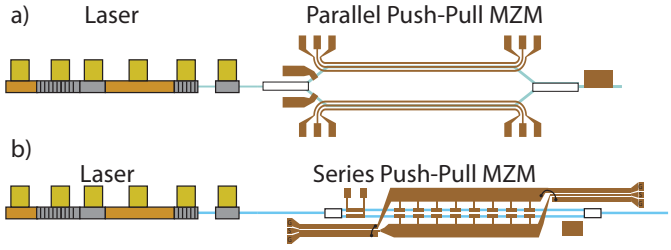

Fig. 2: (a) Tunable transmitter channel with DBR laser and parallel push-pull MZ modulator, requiring two RF in- and two RF outputs. (b) Tunable transmitter with series push-pull modulator, requiring only one RF in- and output.

Fig. 1 shows the transmitter architecture, which is made up from an array of tunable DBR lasers with 100 GHz channel spacing, each laser being connected to a TW-MZM. All eight channels are then combined with a multiplexing arrayed waveguide grating (AWG) into a joint output channel. The choice of DBR lasers is motivated by its small footprint and linear shape which is ideal for parallel transmitter circuits. The choice of the modulator type is influenced by consideration on channel speed, footprint and also its electrical interface. One of the often neglected issues in integrated optical transmitter design is its interface to high-speed electronics. Modulators based on traveling-wave electrodes require a radio-frequency (RF) input connection and a means to terminate the electrode through an integrated load resistor or connect it to an RF output track. To avoid chirp in the modulated output signal, which can impair its transmission performance, tight control of the modulation state is desired and can be achieved through the parallel push-pull configuration as depicted in Fig. 2a [28]. But in this configuration a total of four high-speed RF connections per channel is required and need to be routed towards the edge of the PIC for high-speed wire bond connections to the package or assembly. A large number of high-speed RF interfaces towards a small chip becomes increasingly challenging when the total channel count is scaled up. In order to ease this problem, we utilize a series push-pull modulator instead, shown in Fig. 2b, with a capacitively-loaded electrode structure, that assures both impedance and velocity match so that a modulation speed up to 40 Gbaud can be reached [28]. We reported previously on the co-integration of such modulators with tunable DBR lasers, being a good

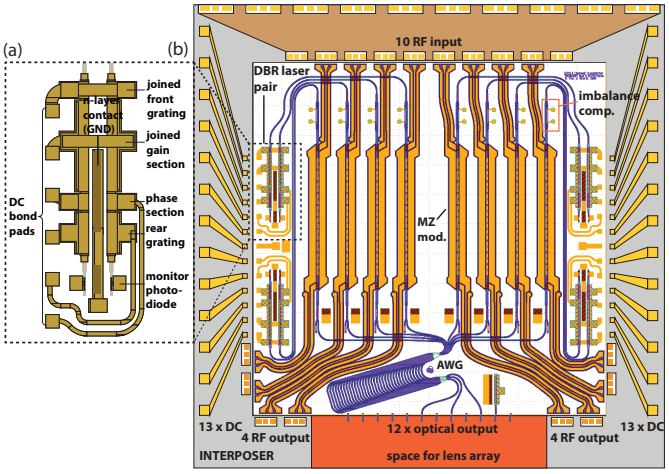

Fig. 3: (a) Layout of the DBR laser pair and (b) complete transmitter layout, which is fully compatible with a proprietary high-speed package. Chip size is 6×6 mm^2

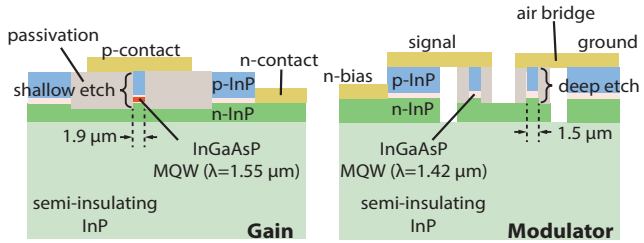

Fig. 4: Integration platform based on semi-insulating InP substrate material and selective multi-quantum well regrowth steps, offering monolithic integration of efficient lasers and EO modulators.

candidate for multi-channel transmitter integration [29]. The RF connection to the capacitively-loaded stripline electrode is made through a broadband coplanar-stripline transition, which is also reported in [29]. Conventional coplanar transmission lines are used to route the signals to the chip edge.

The complete transmitter layout including the 8 DBR lasers and 8 modulators is shown in Fig. 3b. The transmitter circuit is co-designed with a compact, state-of-the-art, high-speed package, also developed in the PARADIGM project, whose electrical interface is overlaid in Fig. 3b with the transmitter layout. An interposer supplies the RF data signals for the 8 modulators from the top through short wire bonds and they exit the transmitter through the bottom side to be terminated into surface-mount resistors. Electrical DC connections for driving lasers, tuning and biasing are supplied through all three sides of the package wall whereas the optical output is on the bottom side of the chip. Owing to the limited number of available DC connections, DBR lasers are grouped into pairs as depicted in Fig. 3a, where both the gain and front grating sections of each laser share the same electrical connection with its neighbor. Sufficient tuneability is still achieved through individual rear grating and phase adjustment sections.

The transmitter contains more than 220 components on a 6×6 mm^2 area and aims at providing an aggregate transmission capacity of 8×40 Gb/s. At the time of writing, the chip is undergoing the packaging procedure and accordingly we only present measurement results obtained from on-chip probing (in section IV) prior to packaging.

The underlying experimental generic platform technology is depicted in Fig. 4, supporting an active-passive integration scheme with multiple regrowth steps to form active multi-quantum wells (MQW) with 1.55 µm band gap for the gain regions and transparent MQWs for the modulator sections. The former is realized with a shallowly etched waveguide whereas the latter is based on a deeply etched waveguide, containing 20 periods of InGaAsP quantum wells at 1.42 µm and barriers at 1.1 µm bandgap so that the electro-optic efficiency is enhanced by the Quantum-Confined Stark Effect. In addition, an air-bridge technology is used to realize the capacitive loading structures in the modulators. A semi-insulating InP substrate is used as the base material to provide sufficient electrical isolation and superior RF performance.

III. Crosstalk Effects and Mitigation

As indicated in the introduction section, the move for transmitter PICs towards higher component density and smaller chip sizes, as a consequence of scaling to more parallel channels and higher capacities, will result in proximity effects that affect the transmitter performance. These fundamental physical coupling mechanisms between neighboring components lead to electrical, thermal and optical crosstalk and are worthwhile investigating. They have gained recent attention in the research community, resulting in several studies [10], [11], [30]–[32]. In this section, we will summarize relevant results from our previous work regarding crosstalk effects in InP transmitters and detail how we applied the insight gained to the demonstrator transmitter design presented in this paper.

A. Radiofrequency Crosstalk

In a high density transmitter, coupling between high-speed RF lines and modulator electrodes can lead to electrical crosstalk noise that is transferred into the optical domain and degrades the transmitter performance. This has been observed for both intensity modulated and phase-intensity modulated signals [32], [33] and we have presented empirical and theoretical relations between electrical crosstalk magnitude and crosstalk penalty [34]. The underlying noise generation mechanisms include radiative, substrate and circuit level crosstalk. In certain cases, when they are well quantified, coherent receivers can successfully compensate their negative effect [35]. If that is not available, possible crosstalk reduction or mitigation techniques have to be considered during the chip design.

As shown in Fig. 5, RF lines with shared ground return electrodes suffer from circuit level ground bounce noise and exhibit a high crosstalk level. A reduction of 20 dB can be achieved by utilizing individual ground return paths [32], which have been adopted in this work for the transmitter design. A separation distance of at least 50 µm needs to be adopted to keep the coupling below -40 dB. Furthermore, the properties of the underlying substrate material, in particular its conductivity and thickness, play an important role in the crosstalk propagation. Fig. 5 depicts the amount of substrate crosstalk experienced by coplanar pad structures as shown in

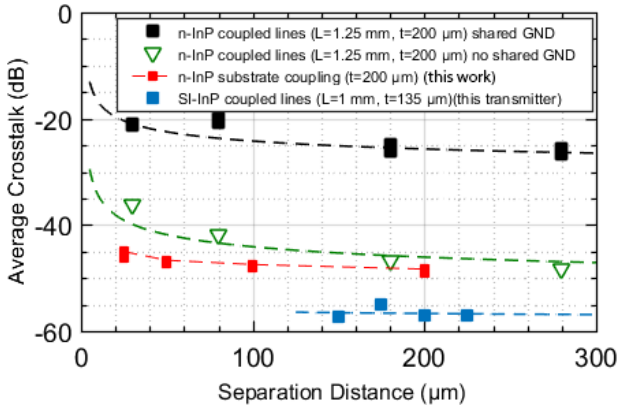

Fig. 5: Measured average crosstalk from DC to 25 GHz for various structures depicted in Fig. 6 at different separation distances. Reduction of RF coupling can be achieved through separation of shared ground returns and the use of semi-insulating substrates.

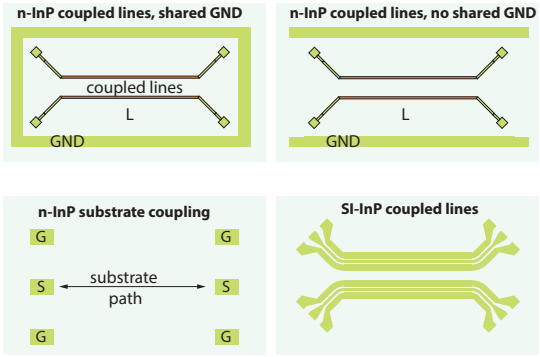

Fig. 6: Types of crosstalk test structures to access the electrical coupling between components.

Fig. 6, which lie on top of a 200 µm thick highly n-doped InP layer ($\sigma = 20000$ S/m). The noise level in this case lies slightly below the coupled line values at around -48 dB because of less radiative coupling. We have also measured coupled coplanar line structures on a semi-insulating substrate, which show a further reduction in crosstalk of around 10 dB. This suggests that the insulating property of the substrate is effective in reducing electrical coupling.

To have more insight into the substrate noise generation and propagation mechanisms a simple equivalent circuit can be used, consisting of two pads with assumed 0.3 fF coupling, separated from the InP substrate by a thin dielectric layer, as depicted in Fig. 7 [36]. Crosstalk noise is injected by means of the dielectric layer capacitance from pad A into the substrate and can propagate to pad B through a resistive network and picked up again by a capacitive mechanism. Fig. 7a shows the influence of the substrate conductivity on the calculated crosstalk for a fixed thickness value whereas Fig. 7b depicts the influence of the substrate thickness in case of an n-doped and semi-insulating substrate. It can be observed that crosstalk noise is very sensitive to substrate conductivity and peaks at around 1000 S/m. For an n-doped substrate ($\sigma \approx 20000$ S/m) the doping concentration then determines the amount of substrate noise, whereas in case of a semi-

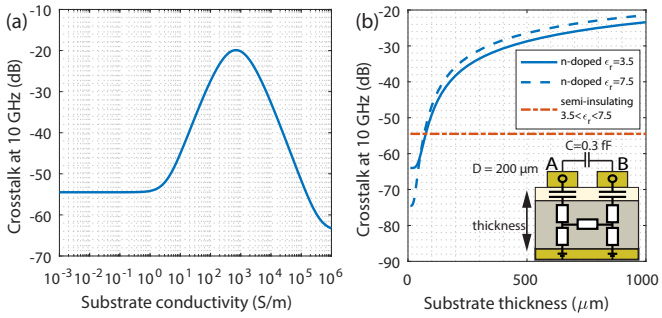

Fig. 7: A simple two layer model with a 260 nm thick layer mimicking a range of dielectric materials and a 200 µm thick substrate layer is used to illustrate its effect on the RF crosstalk. (a) Calculated RF coupling at 10 GHz and D=200 µm, $\epsilon_r = 3.5$, for substrate equivalent circuit shown in (b) when the substrate conductivity is varied. (b) Calculated RF crosstalk when substrate thickness is varied for n-doped ($\sigma = 20000$ S/m) and semi-insulating ($\sigma = 10^{-5}$ S/m) material. Equivalent circuit for substrate crosstalk with A and B representing 50×75 μm^2 contact pads with 0.3 fF coupling.

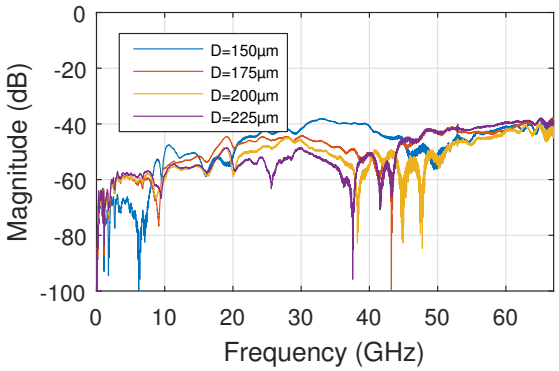

Fig. 8: Crosstalk between coupled coplanar RF lines of 1 mm length on semi-insulating substrate with varying separation distances D. Low RF coupling is attributed to the isolation properties of the substrate

insulating substrate ($\sigma = 10^{-5}$ S/m), the coupling can be held very low due to small conductivity values. The constant crosstalk at low substrate conductivity in Fig. 7a is given by the assumed background capacitive coupling. Fig. 7b indicates that substrate thinning can be effective for n-doped substrates to reduce crosstalk whereas the same does not apply for semi-insulating substrates. For our given sample with 135 µm thick semi-insulating material, the modeled results are around -55 dB and can be compared to the measurements.

The transmitter presented in this paper is fabricated on a semi-insulating substrate with 135 µm thickness, yielding a very low amount of electrical crosstalk. Measurements depicted in Fig. 8 of 1 mm long coupled RF lines at varying separation distances show that the coupling is below -40 dB up until 67 GHz. According to results in [32] this amount of crosstalk leads to a negligible amount of transmission power penalty. The actual spacing of RF lines and modulator electrodes between adjacent channels is kept at 500 µm in the transmitter design to eliminate radiative coupling and guarantee that crosstalk stays below -40 dB. An interesting ob-

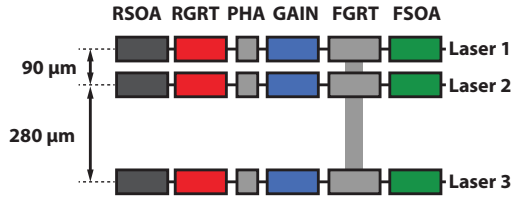

Fig. 9: Illustration of DBR laser array that was used to quantify the amount of thermal crosstalk, typical to InP based PICs.

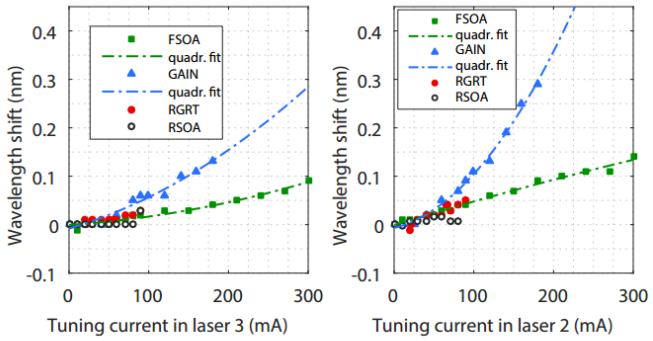

(a) (b)

Fig. 10: (a) Thermal crosstalk induced wavelength shift on laser 1 from laser 3. (b) Induced wavelength shift on laser 1 from laser 2.

servation here is that for the current technology, the minimum separation between RF lines is constrained by the dimensions of the metal bond pads rather than the coupling crosstalk. We will elaborate this point in more detail in section IV on scalability issues.

B. Thermal Crosstalk

A second important proximity effect is thermal crosstalk which occurs between laser sections. Resistive Joule heating in lasers is well known to reduce the efficiency and output power. In addition, local temperature rise leads to a change in refractive index and results in undesired wavelength drift. Substantial efforts have been made to reduce the series resistance of laser devices and to make them more resilient to temperature increase, such as using Al-containing gain material [37]. However, a residual access resistance always remains in p-i-n based ridge-waveguide laser structures due to the use of p-dopants, resulting in device resistances in the range of several Ohm. Therefore, heating of lasers under strong current injection will continue to be a problem for densely integrated arrays and appropriate ways to deal with it are needed for the design of parallel transmitters.

We have previously studied the performance of an array of DS-DBR lasers under the influence of thermal crosstalk that occurs between them [38]. Here we show extended measurements which give a more detailed view on the effect of thermal crosstalk for two laser separation distances. Fig. 9 shows the schematic illustration of the measured laser array where laser 2 and laser 3 are separated from laser 1 by 90 and 280 µm respectively. In our test, the wavelength of laser 1 is tracked

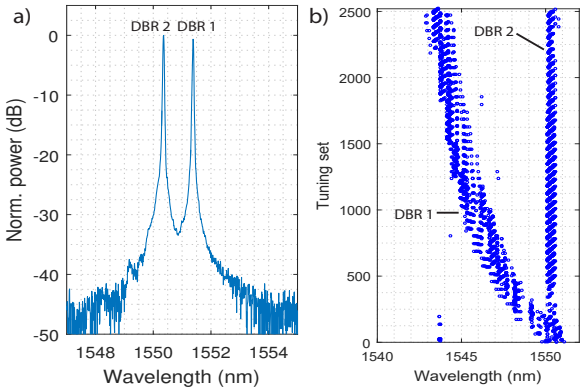

Fig. 11: (a) Spectrum of a laser pair when both are simultaneously operated. (b) Individual tuning of one laser in the pair through a combination of front and rear grating adjustments. Both lasers share the same front grating electrode due to packaging constraints.

when sections of the adjacent lasers are tuned individually, so that their thermal crosstalk effect can be quantified. Fig. 10 shows the measurement results, from which it can be observed that the active sections, in this case gain and booster SOAs, contribute the most to thermal crosstalk. At typical current injection values of 100 mA the maximum wavelength shift is below 0.05 nm for a separation of 280 µm and increases to 0.1 nm when the distance between both lasers shrinks to 90 µm. As the main operation principle of DBR lasers used for this work do not inherently differ to that of DS-DBR lasers, we use that measurement data as a guideline for specifying laser design rules for our parallel transmitter. With 100 GHz channel spacing, a 0.1 nm temperature induced shift would be still acceptable for 40 GHz modulation bandwidth, which imposes a minimum separation distance of 90 µm between adjacent laser devices. In this work, we choose a separation of 160 µm to account for some tolerances.

In addition, we demonstrated that by including fine phase adjustment sections into the DS-DBR laser cavity, the temperature induced wavelength shifts can be compensated for and exact alignment to ITU wavelength grid is possible even under simultaneous array operation and thermal crosstalk [38]. Therefore, phase tuning sections have also been included for the DBR lasers in this work. In fact, measurements on DBR laser pairs of the fabricated transmitter device show that individual tuning of one of the lasers can be achieved when both are simultaneously operated. Fig. 11 depicts the spectrum and its evolution of a DBR laser pair. It can be seen, that the wavelength of laser 1 is separately tuned in a range of 8 nm. Here, a tuning set consists of a specific pair of front and rear grating currents that are applied to yield the desired wavelength. The small variation in laser 2 wavelength is caused by the fact, that the front grating contacts of both lasers are connected together as discussed in section II and therefore any tuning there affects both lasers. This can however, be easily compensated by phase adjustments of laser 2.

In this section, we have depicted how spacing rules can be established from calibration measurements and how they can

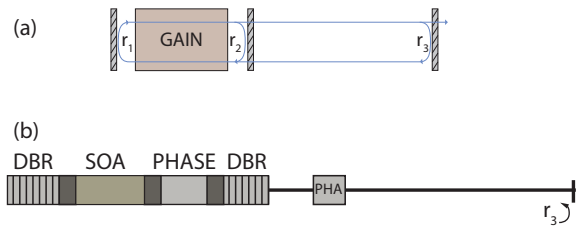

Fig. 12: (a) Fabry-Perot laser with feedback. (b) Schematic showing a DBR laser with external cavity phase control section for suppressing relaxation oscillations due to external weak feedback.

be successfully used on the design of parallel transmitters, leading to the fabrication of laser arrays that are less affected by thermal crosstalk.

C. Optical Crosstalk

In a high-density photonic circuit such as a parallel transmitter, spurious reflections of the optical signals can occur at component interfaces such as inputs to couplers, splitters and waveguide transitions, or at the facets of the chip. These reflections, although small in magnitude, can find their way back to the tunable laser source and cause detrimental effects [39]. Therefore, it is necessary to study the behavior of the laser under the influence of small reflections, also known as feedback. The literature has focused on this topic already since the beginning of the semiconductor laser and contains many studies on the effect of weak optical feedback [39]–[42]. Stable lasing operation can be perturbed to transition into different types of unstable operation or regimes depending on the strength of the feedback light [43]. If the spurious reflection occurs after an optical modulator, the feedback light will be varied in its amplitude, as it passes twice the modulation. This can cause additional laser chirping and has been analyzed in case of electro-absorption [44] and Mach-Zehnder modulators [45] before. Rigorous modeling of such large-signal effects needs however to account for the time-dependent feedback light in the entire transmitter network and becomes more difficult with an increasing number of components. Here, we present our initial investigation on feedback in the transmitter design, accounting for a single continuous-wave reflection that is not modulated, as this simple reflection already can cause instabilities in form of undamped relaxation oscillations (RO). Recent experimental work has emphasized the importance of the feedback phase in this case and it has been shown in [46] that by tightly controlling it, the undamped RO can be suppressed again. Proper phase control can in circumstances also work advantageous in case of modulated feedback as was shown in [47]. In this section, we present a numerical study on the importance of feedback phase for conditions similar to the ones occurring in our transmitter chip.

Fig. 12a depicts a Fabry-Perot cavity with an external reflection r_3 representing the source of feedback and is a simplified description of a single spurious reflection into the laser in case of the parallel transmitter. Such a model can be described by a rate equation system including terms for the delayed feedback field, also called Lang-Kobayashi

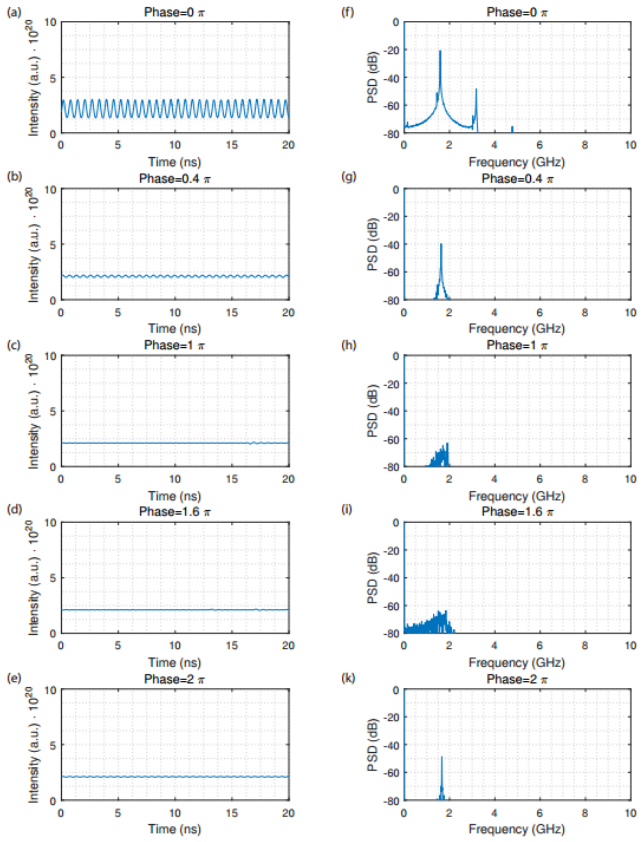

Fig. 13: Numerical simulation results of the influence of the feedback phase on laser operation (-25 dB power reflection). The feedback phase is increased from 0 to 2π and the time and frequency domain representation of the laser output intensity is shown in (a)-(e) and (f)-(k) respectively.

equations [48] (given in the Appendix). We have followed the approach in [49] and performed numerical simulations for laser parameters corresponding to our platform and device geometry. The DBR laser is approximated by a Fabry-Perot cavity using the effective length and reflectivity values of the gratings. As an example, we set the feedback strength to -25 dB, which approximately matches the reflection of a typical MMI coupler in comparable technologies [50], and compute the steady-state solutions to the Lang-Kobayashi equations in order to obtain the intensity output trace of the laser. Fig. 13a and f depict the time and frequency domain representation of the laser's output intensity under feedback, showing an undamped relaxation oscillation behavior with a dominant frequency at 1.5 GHz. The frequency domain is given by the power spectral density (PSD) of the time-domain trace. The visible oscillation arises due to the interaction of the feedback light with carrier dynamics, building a positive feedback loop, and is well understood in theory and experiment [51]. We extend the model to include the effect of an external cavity phase shifter that can change the feedback phase. Such a control mechanism can readily be integrated with DBR lasers, as shown schematically in Fig. 12b, and measurements on a fabricated device indicated suppression of the RO under feedback [52]. By slowly increasing the extra phase change

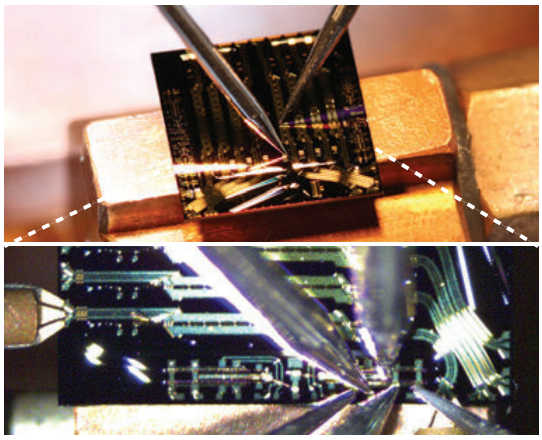

Fig. 14: Photograph of the transmitter PIC under test using DC and RF probes and lensed fiber coupling.

to the feedback signal, the RO is also suppressed in our simulations, as Fig. 13b-e and g-k show. At π additional phase change, the laser output reverts to a stable operation, indicating the effectiveness of this technique. If the additional phase change is further increased, at some point the RO reappears, so the exact amount of phase change is a critical aspect of the control mechanism. The results indicate that in practical transmitter designs, the use of an external cavity phase control is a useful addition to the laser design for controlling its behavior in possible feedback conditions.

After elaborating in detail our considerations to the chip design with respect to crosstalk effects and how those affect the transmitter performance, we continue to present the measurement results of the fabricated device in the next section.

IV. High-Capacity Transmitter

A. Transmitter Performance

As indicated in section II, the transmitter electrical and optical interfaces have been designed to match an existing high-speed package. After fabrication of the PIC device, we have characterized its performance using direct probing with DC and RF probes and extracting the optical signal with a lensed fiber from the joint chip output facet. Fig. 14 shows a photograph of the transmitter chip under test, on top of a temperature controlled stage which is held at 15° C. A typical laser LI and IV curve is shown in Fig. 15, indicating low threshold currents at 13 mA and up to several mW of output power in fiber. These results have been measured on test lasers from an adjacent cell of the same wafer as the lasers of the actual transmitter are placed before the modulator and AWG so that their outputs are not directly accessible. Each DBR laser can be tuned in a 9-10 nm range and therefore can be aligned to their respective WDM channel passbands. Fig. 16 shows the spectral output of the transmitter for all 8 channels with the AWG passbands overlaid. Typical SMSR values exceed 40 dB. All 8 modulator devices show consistent DC switching performance in Fig. 17 with half-wave voltages as low as 1.5 V. The measurement was performed with a common mode bias of 11.5 V.

Furthermore, we characterized the dynamic performance of the transmit channels by measuring the EO frequency response

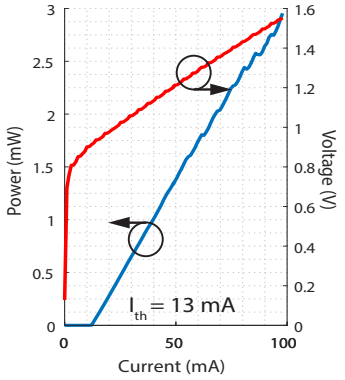

Fig. 15: Typical IV and LI curve measured on DBR laser with direct output to chip facet.

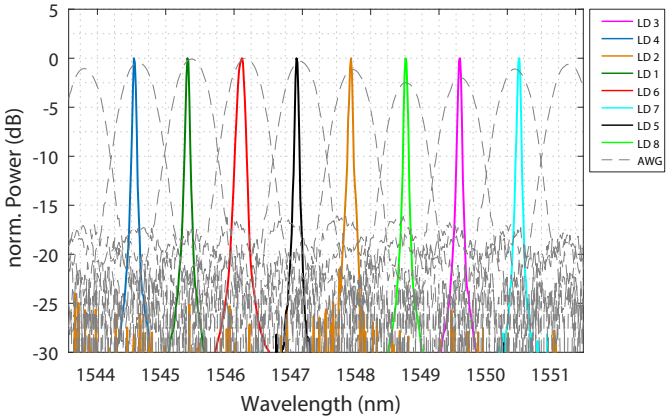

Fig. 16: Spectrum showing all eight DBR lasers aligned to ITU grid wavelengths with the output AWG passbands overlayed.

curves as shown in Fig. 18 with a 67 GHz Agilent Lightwave Component Analyzer. The 3 dB bandwidth of the 2 mm long modulators ranges from 34 to 41 GHz which is sufficient for 40 Gb/s intensity modulation and the return loss stays below 10 dB over the entire frequency range. The variation in EO frequency response between channels is caused by a small problem in the air-bridge definition, leading to varying access resistance values for the modulator phase shift sections. This processing issue has since been solved and we expect that future fabrication of the same device will show uniform

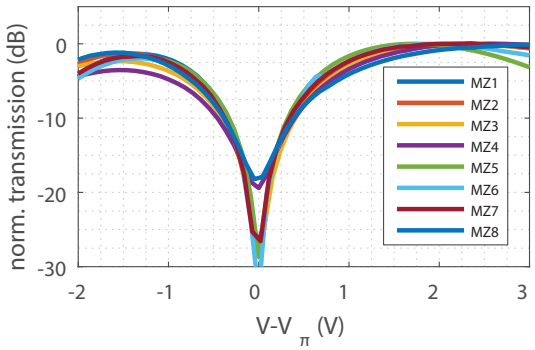

Fig. 17: Measured DC switching curves of all eight modulators. A low V_π of 1.5 V can be observed at 11.5 V common mode bias.

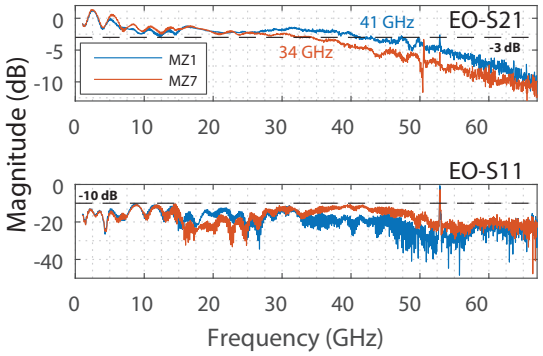

Fig. 18: EO-frequency response measurements of two exemplary channels showing bandwidth up to 40 GHz and <10 dB return loss.

resistances.

To assess the modulation characteristics, we performed large-signal modulation on each channel separately by operating the laser at its respective WDM wavelength and biasing the modulators to 10 V common mode Voltage and applying a 2 V drive signal at 30 and 40 Gb/s on-off-keying. Fig. 19 shows the received optical eye diagrams at back-to-back transmission for both bit rates and the initial electrical input signal. We can observe clear eye openings at 30 Gb/s which start to close at 40 Gb/s. This is partially caused by the bandwidth limitations of the driving amplifier (35 GHz) and cables, which led to a degraded electrical input signal. The differences between channels can be attributed to the same processing issue as discussed earlier regarding air-bridges. During the characterization, channel 1 was damaged so that it could not be characterized at 30 Gb/s anymore. After reception of the modulated signals, we performed bit-error-rate (BER) measurements which are depicted in Fig. 20a and b. The better-performing channels lead to error-free detection at 30 Gb/s and with the air-bridge issue resolved, all channels will achieve this performance. At 40 Gb/s an error floor at 10^{-4} is evident but the BER is below the hard-decision forward-error correction threshold, so that by sacrificing FEC overhead, error-free operation can be achieved. In addition, we transmitted the modulated output signal at 20 Gb/s through 20 km of single mode fiber to illustrate the feasibility of the transmitter for medium-reach applications and could obtain error-free detection. Fig. 20c shows the BER curves in this case and the eye diagram before and after the fiber span. The result also confirms that chirp is kept low due to the series push-pull driving scheme applied in this transmitter.

Due to the nature of the direct-probing test setup and a lack of probing space, simultaneous dynamic operation of multiple channels could not be performed, so that the dynamic effect of possible electrical crosstalk has not been characterized. From our measurements presented in section III, however, we are confident that electrical crosstalk is kept at a low level in the fabricated transmitter.

We have presented static and dynamic characterization results of the fabricated parallel transmitter so far, showing that it is capable of providing 8×40 Gb/s capacity or after FEC overhead a total of 300 Gb/s capacity on a compact 6×6 mm^2 area and enough wavelength tuneability to address 8 WDM channels. By applying design rules that take crosstalk effects into account, the present device exhibits high integration density with minimal proximity effects occurring between transmit channels. In the final section, we will focus on the scalability and future prospects of parallel transmitters in generic integration technologies.

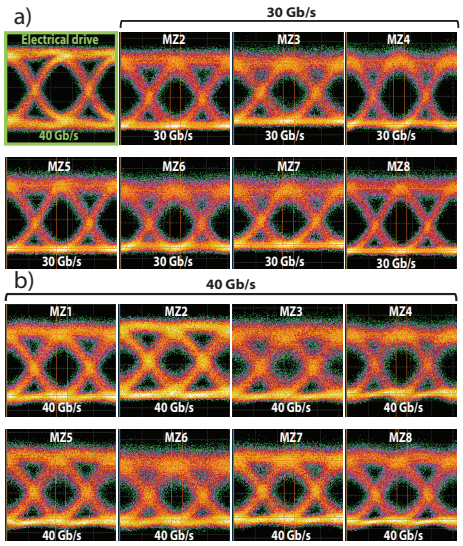

Fig. 19: (a) Large signal modulation eye diagrams at 30Gb/s and (b) at 40Gb/s.

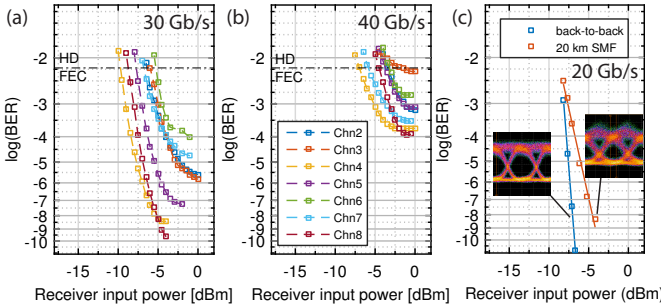

Fig. 20: (a) received BER at 40Gb/s and (b) at 30Gb/s OOK in back-to-back configuration and (c) at 20Gb/s after transmission through 20 km SMF.

B. Prospects and Scalability

It is worthwhile making the comparison between the transmitter from this work and previously published examples from literature. One of the often presented metrics is the number of components per chip for PIC devices, which has been shown to increase exponentially for the general case of InP integrated photonics [9]. In case of high-capacity transmitter circuits, we can evaluate the capacity per chip metric and a similar trend is visible as shown in Fig. 21a, where the data from [8] has been extended with recently published results [3], [25], [53]–[58]. It shows that generic technology platforms are still behind in terms of pure capacity per chip compared to very specialized product platforms for the telecom and datacom industry but that they also show an exponential growth trend. In terms of integration density, a more useful metric is to normalize the plot to the chip area, which is shown in Fig. 21b, because the goal is to maximize capacity and at the same time

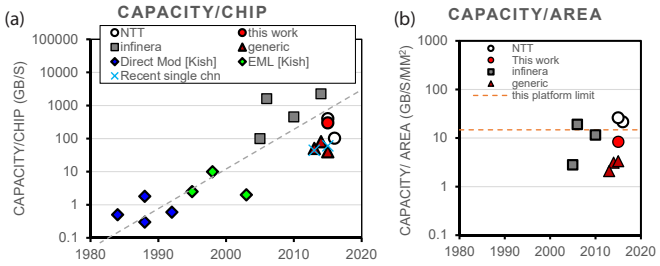

Fig. 21: (a) Comparison of transmitter capacities normalized to per chip and (b) per unit area with indication of this platform's limit.

minimize chip area. Here, we see that the presented work is comparable with other state-of-the-art demonstrators from the industry at around 10 Gb/s/mm^2. This metric in the presented transmitter is limited by the laser and modulator separation of 160 μm and 500 μm. If the minimum values for acceptable thermal and electrical crosstalk of 90 μm and 50 μm are taken, each transmit channel would occupy less space and the metric can be increased to 14.8 Gb/s/mm^2. In that case, the modulator electrode and RF interconnect size is the limiting factor on the chip. We expect the metric to increase further, if advanced modulation formats are used in transmitters from generic platforms with higher spectral efficiencies.

We have discussed the limitations of electrical and thermal crosstalk effects on the component separation in the presented transmitter so far. Another major limitation to further scaling towards higher integration density is found in the packaging solution for the PIC. In this case, we utilize a conventional gold box package with wire bond connections. This represents a one-dimensional interface to the photonic circuit. As scaling towards smaller chip sizes and more parallel channels is inherently two-dimensional, this packaging solution cannot keep up with future scaling trends. We have seen how bond pad placement already limits the device distances on the chip so that more advanced interconnection technologies are needed in future parallel transmitter PICs. In contrast, flip-chip bonding of transmitter to an interposer or electronic IC [59]–[61] can achieve a two-dimensional interface. Another promising approach is wafer-scale bonding of InP photonic circuits with electronics, which is currently being investigated [62]. To sustain continued scaling of integrated parallel optical transmitters towards higher capacities, advancements in the chip packaging and interconnect technology are necessary and proper management of crosstalk effects is essential, the latter being the main focus in this work.

V. Conclusion

InP based PIC technology remains a strong candidate for high-density parallel optical transmitters that are needed for future high-capacity datacom and telecom applications, due to the advantages in large-scale integration of active and passive components, small device foot-print due to high integration density and the availability of efficient and high-speed components. Generic photonic integration platforms provide low cost access and offer easy design and manufacturing routes with excellent performance. We demonstrated this by realizing a parallel transmitter circuit fabricated in an experimental generic platform. This circuit is capable of 300 Gb/s total transmit capacity with almost 10 Gb/s/mm^2 capacity density. This was enabled by developing a crosstalk-resilient design which reduces undesired proximity effects in the fabricated device. We analyzed the influence of electrical, thermal and optical crosstalk effects that can degrade the transmitter performance and indicated mitigation methods, yielding a compact, high-density chip. The demonstrator operates with an IM/DD scheme but the same principles can readily be applied to devices for advanced modulation formats using nested IQ modulator architectures. The insight into physical crosstalk mechanisms gained in this work will also apply for more advanced transmitter architectures and is helpful for continued scaling of integrated parallel transmitters towards Tb/s capacities.

VI. Appendix

In section III-C we use the Lang-Kobayashi equations to model weak optical feedback effects to the laser operation. They have the form

$$\frac{d\mathbf{E}(t)}{dt} = \frac{1+i\alpha}{2}\left[G_N\left(N(t)-N_0\right) - \frac{1}{\tau_p}\right]\mathbf{E}(t) + \kappa\mathbf{E}(t-\tau_{ext})e^{-i\omega_{th}\tau_{ext}} \quad (1)$$

$$\frac{dN(t)}{dt} = J - \frac{N(t)}{\tau_s} - G_N\left(N(t)-N_0\right)\left|\mathbf{E}(t)\right|^2, \quad (2)$$

with slowly varying envelope function $\mathbf{E}(t)$ of the electric field and the carrier density $N(t)$ in the gain material. The lasing frequency of the laser without feedback at threshold is ω_{th}. The feedback strength is represented with the factor

$$\kappa = \frac{1}{\tau_{int}}\frac{(1-r_2^2)r_3}{r_2}. \quad (3)$$

The round trip times of internal (τ_{int}) and external (τ_{ext}) cavities are calculated from the effective index n_{eff} and light velocity c through $\tau = 2n_{eff}L/c$. The remaining parameters are the gain coefficient G_N, transparency carrier density N_0, photon and carrier lifetimes τ_p and τ_s, linewidth enhancement α and injection current density J and have been taken from [63].

Acknowledgment

We thank Oclaro Technology Ltd, Caswell, UK, for collaboration and for fabrication of the devices in their experimental generic platform. This work was supported by the Dutch STW project ELPHI (11354) and the EC Framework 7 project PARADIGM (257210). We thank Prof. Daan Lenstra for fruitful discussions.

References

[1] "Integrated Optical Devices - Is Silicon Photonics a Disruptive Technology?" *LightCounting Market Research*, Jan. 2016.

[2] M. Smit, X. Leijtens, H. Ambrosius *et al.*, "An introduction to InP-based generic integration technology," *Semicond. Sci. Technol.*, vol. 29, no. 8, p. 083001, Jun. 2014.

[3] K. Lawniczuk, C. Kazmierski, J. Provost *et al.*, "InP-Based Photonic Multiwavelength Transmitter With DBR Laser Array," *IEEE Photonics Technology Letters*, vol. 25, no. 4, pp. 352–354, Feb. 2013.

[4] S. Stopinski, M. Malinowski, R. Piramidowicz *et al.*, "Monolithically integrated 8-channel WDM reflective modulator," in *Optical Fiber Communication Conference (OFC), 2013*, Mar. 2013, p. OW4J.7.

[5] W. Forysiak and D. S. Govan, "Progress Toward 100-G Digital Coherent Pluggables Using InP-Based Photonics," *Journal of Lightwave Technology*, vol. 32, no. 16, pp. 2925–2934, Aug. 2014.

[6] V. Lal, J. Summers, A. Hosseini *et al.*, "Full C-Band Tunable Coherent Transmitter and Receiver InP Photonic Integrated Circuits," in *42nd European Conference on Optical Communication (ECOC), PDP, 2016*, Sep. 2016, pp. 1–3.

[7] D. A. B. Miller, "Attojoule Optoelectronics for Low-Energy Information Processing and Communications," *Journal of Lightwave Technology*, vol. 35, no. 3, pp. 346–396, 2017.

[8] F. Kish, R. Nagarajan, M. Missey *et al.*, "Current Status of Large-Scale InP Photonic Integrated Circuits," *IEEE Journal of Selected Topics in Quantum Electronics*, vol. 17, no. 6, pp. 1470 –1489, Nov.-Dec. 2011.

[9] M. Smit, J. van der Tol, and M. Hill, "Moore's law in photonics," *Laser & Photonics Reviews*, vol. 6, no. 1, pp. 1–13, 2012.

[10] D. Melati, F. Morichetti, G. G. Gentili *et al.*, "Optical radiative crosstalk in integrated photonic waveguides," *Opt. Lett.*, vol. 39, no. 13, pp. 3982–3985, Jul. 2014.

[11] W. Yao, G. Gilardi, N. Calabretta *et al.*, "Experimental and Numerical Study of Electrical Crosstalk in Photonic Integrated Circuits," *Journal of Lightwave Technology*, vol. 33, no. 4, pp. 934–942, Feb. 2015.

[12] G. Gilardi, W. Yao, M. K. Smit *et al.*, "Observation of Dynamic Extinction Ratio and Bit Error Rate Degradation Due to Thermal Effects in Integrated Modulators," *Journal of Lightwave Technology*, vol. 33, no. 11, pp. 2199–2205, Jun. 2015.

[13] W. Yao, M. K. Smit, and M. J. Wale, "Monolithic 8 x 40 Gb/s Tunable WDM Transmitter Based on Generic III-V Technology," in *Conference on Lasers and Electro-Optics (2017), Paper SM4O.3*. Optical Society of America, May 2017, p. SM4O.3.

[14] R. Nagarajan, C. Joyner, J. Schneider, R.P. *et al.*, "Large-scale photonic integrated circuits," *IEEE Journal of Selected Topics in Quantum Electronics*, vol. 11, no. 1, pp. 50 – 65, jan.-feb. 2005.

[15] A. H. Gnauck and P. J. Winzer, "Optical phase-shift-keyed transmission," *Journal of Lightwave Technology*, vol. 23, no. 1, pp. 115–130, Jan. 2005.

[16] P. J. Winzer and R.-J. Essiambre, "Advanced Modulation Formats for High-Capacity Optical Transport Networks," *J. Lightwave Technol., JLT*, vol. 24, no. 12, pp. 4711–4728, Jan. 2006.

[17] R. Nagarajan, C. Doerr, and F. Kish, *Optical Fiber Telecommunications VIA: Chapter 2. Semiconductor Photonic Integrated Circuit Transmitters and Receivers*. Elsevier Inc., May 2013.

[18] R. A. Griffin, S. K. Jones, N. Whitbread *et al.*, "InP Mach-Zehnder Modulator Platform for 10/40/100/200-Gb/s Operation," *IEEE Journal of Selected Topics in Quantum Electronics*, vol. 19, no. 6, pp. 158–166, Nov. 2013.

[19] R. A. Griffin, N. D. Whitbread, S. Jones *et al.*, "InP Coherent Optical Modulator with Integrated Amplification for High Capacity Transmission," in *Optical Fiber Communication Conference (2015)*. Optical Society of America, Mar. 2015, p. Th4E.2.

[20] R. J. Essiambre, G. Kramer, P. J. Winzer *et al.*, "Capacity Limits of Optical Fiber Networks," *Journal of Lightwave Technology*, vol. 28, no. 4, pp. 662–701, Feb. 2010.

[21] J. H. Sinsky and P. J. Winzer, "100-Gb/s optical communications," *IEEE Microwave Magazine*, vol. 10, no. 2, pp. 44–57, Apr. 2009.

[22] Y. Ogiso, J. Ozaki, Y. Ueda *et al.*, "Over 67 GHz Bandwidth and 1.5 V Vπ InP-Based Optical IQ Modulator With n-i-p-n Heterostructure," *Journal of Lightwave Technology*, vol. 35, no. 8, pp. 1450–1455, Apr. 2017.

[23] P. J. Winzer and D. T. Neilson, "From Scaling Disparities to Integrated Parallelism: A Decathlon for a Decade," *Journal of Lightwave Technology*, vol. 35, no. 5, pp. 1099–1115, Mar. 2017.

[24] P. J. Winzer, "Making spatial multiplexing a reality," *Nat Photon*, vol. 8, no. 5, pp. 345–348, May 2014.

[25] S. Kanazawa, T. Fujisawa, H. Ishii *et al.*, "High-Speed (400 Gb/s) Eight-Channel EADFB Laser Array Module Using Flip-Chip Interconnection Technique," *IEEE Journal of Selected Topics in Quantum Electronics*, vol. 21, no. 6, pp. 183–188, Nov. 2015.

[26] Photonic Advanced Research And Development for Integrated Generic Manufacturing, "PARADIGM - Final publishable summary report," european Commision FP7-ICT-2009-5.

[27] J. Renaudier, R. Rios-Müller, M. A. Mestre *et al.*, "Multi rate IMDD transceivers for optical interconnects using coded modulation," in *2016 Optical Fiber Communications Conference and Exhibition (OFC)*, Mar. 2016, p. Tu2J.2.

[28] R. Walker, "High-speed III-V semiconductor intensity modulators," *IEEE Journal of Quantum Electronics*, vol. 27, no. 3, pp. 654 –667, Mar. 1991.

[29] W. Yao, M. K. Smit, and M. J. Wale, "Monolithically Integrated 40 Gbit/s Tunable Transmitter in an Experimental Generic Foundry Process for Large-Scale Integration," in *42nd European Conference on Optical Communication (ECOC), 2016*, Sep. 2016, pp. 1–3.

[30] T. Umezawa, T. Angkaew, and T. Kawanishi, "Data rate penalty for high-density photonic integrated circuits in advanced modulation formats," in *2014 International Topical Meeting on Microwave Photonics (MWP) and the 2014 9th Asia-Pacific Microwave Photonics Conference (APMP)*, Oct. 2014, pp. 142–145.

[31] T. Angkaew, T. Umezawa, and T. Kawanishi, "Crosstalk reduction for large scale photonic integrated circuits," in *2014 International Topical Meeting on Microwave Photonics (MWP) and the 2014 9th Asia-Pacific Microwave Photonics Conference (APMP)*, Oct. 2014, pp. 131–134.

[32] W. Yao, G. Gilardi, M. K. Smit *et al.*, "Performance Degradation of Integrated Optical Modulators Due to Electrical Crosstalk," *Journal of Lightwave Technology*, vol. 34, no. 13, pp. 3080–3086, Jul. 2016.

[33] P. J. Winzer, A. H. Gnauck, A. Konczykowska *et al.*, "Penalties from in-band crosstalk for advanced optical modulation formats," in *2011 37th European Conference and Exhibition on Optical Communication*, Sep. 2011, p. Tu.5.B.7.

[34] W. Yao, M. K. Smit, and M. J. Wale, "Intuitive analytical model relating electrical crosstalk in Mach-Zehnder modulators to performance degradations," in *Proceedings of the 21st Annual Symposium of the IEEE Photonics Society Benelux Chapter*, Gent, Belgium, November 17-18, 2016, pp. 15 – 18.

[35] X. Chen, P. Dong, S. Chandrasekhar *et al.*, "Characterization and Digital Pre-compensation of Electro-optic Crosstalk in Silicon Photonics I/Q Modulators," in *42nd European Conference on Optical Communication (ECOC), 2016*, Sep. 2016, pp. 1–3.

[36] X. Aragones and A. Rubio, "Challenges for signal integrity prediction in the next decade," *Materials Science in Semiconductor Processing*, vol. 6, no. 1–3, pp. 107–117, Feb. 2003.

[37] J. Piprek, J. K. White, and A. J. SpringThorpe, "What limits the maximum output power of long-wavelength AlGaInAs/InP laser diodes?" *IEEE Journal of Quantum Electronics*, vol. 38, no. 9, pp. 1253–1259, Sep. 2002.

[38] W. Yao, G. Gilardi, M. K. Smit *et al.*, "Simultaneous full C-band tuning of three integrated DS-DBR lasers in presence of strong thermal crosstalk," in *2015 European Conference on Lasers and Electro-Optics - European Quantum Electronics Conference (2015), Paper CI_2_6*, Jun. 2015, p. CI_2_6.

[39] D. Lenstra, B. Verbeek, and A. D. Boef, "Coherence collapse in single-mode semiconductor lasers due to optical feedback," *IEEE Journal of Quantum Electronics*, vol. 21, no. 6, pp. 674–679, Jun. 1985.

[40] N. Schunk and K. Petermann, "Measured feedback-induced intensity noise for 1.3 mu m DFB laser diodes," *Electronics Letters*, vol. 25, no. 1, pp. 63–64, Jan. 1989.

[41] J. Helms, C. Kurtzke, and K. Petermann, "External feedback requirements for coherent optical communication systems," *Journal of Lightwave Technology*, vol. 10, no. 8, pp. 1137–1141, Aug. 1992.

[42] K. Petermann, "External optical feedback phenomena in semiconductor lasers," *IEEE Journal of Selected Topics in Quantum Electronics*, vol. 1, no. 2, pp. 480–489, Jun. 1995.

[43] R. Tkach and A. Chraplyvy, "Regimes of feedback effects in 1.5 - .mm distributed feedback lasers," *Journal of Lightwave Technology*, vol. 4, no. 11, pp. 1655–1661, Nov. 1986.

[44] P. D. Pukhrambam, S. L. Lee, and G. Keiser, "Electroabsorption Modulated Lasers With High Immunity to Residual Facet Reflection by Using Lasers With Partially Corrugated Gratings," *IEEE Photonics Journal*, vol. 9, no. 2, pp. 1–16, Apr. 2017.

[45] X. Li, W. P. Huang, D. M. Adams *et al.*, "Modeling and design of a DFB laser integrated with a Mach-Zehnder modulator," *IEEE Journal of Quantum Electronics*, vol. 34, no. 10, pp. 1807–1815, Oct. 1998.

[46] J. Zhao, D. Lenstra, R. Santos *et al.*, "Feedback Phase Influence on an Integrated Filtered-Feedback Laser," *IEEE Photonics Technology Letters*, vol. 24, no. 23, pp. 2195–2197, Dec. 2012.

[47] S. F. Yu and N. Q. Ngo, "Simple model for a distributed feedback laser integrated with a Mach-Zehnder modulator," *IEEE Journal of Quantum Electronics*, vol. 38, no. 8, pp. 1062–1074, Aug. 2002.

[48] R. Lang and K. Kobayashi, "External optical feedback effects on semiconductor injection laser properties," *IEEE Journal of Quantum Electronics*, vol. 16, no. 3, pp. 347–355, Mar. 1980.

[49] A. Uchida, "Analysis of Chaotic Laser Dynamics: Example of Semiconductor Laser with Optical Feedback," in *Optical Communication with*

Chaotic Lasers. Wiley-VCH Verlag GmbH & Co. KGaA, 2012, pp. 145–210.
[50] E. Kleijn, D. Melati, A. Melloni *et al.*, "Multimode Interference Couplers With Reduced Parasitic Reflections," *IEEE Photonics Technology Letters*, vol. 26, no. 4, pp. 408–410, Feb. 2014.
[51] J. Zhao, D. Lenstra, R. Santos *et al.*, "Stability of a monolithic integrated filtered-feedback laser," *Optics Express*, vol. 20, no. 26, p. B270, Dec. 2012.
[52] D. D'Agostino, H. Ambrosius, M. Smit *et al.*, "Integrated Laser With Optical Feedback Shows Suppressed Relaxation-Oscillation Dynamics," *IEEE Photonics Technology Letters*, vol. 27, no. 21, pp. 2292–2295, Nov. 2015.
[53] J. Summers, T. Vallaitis, P. Evans *et al.*, "Monolithic inp-based coherent transmitter photonic integrated circuit with 2.25 Tbit/s capacity," *Electronics Letters*, vol. 50, no. 16, pp. 1150–1152, Jul. 2014.
[54] S. Kanazawa, W. Kobayashi, Y. Ueda *et al.*, "30-km Error-Free Transmission of Directly Modulated DFB Laser Array Transmitter Optical Sub-Assembly for 100-Gb Application," *Journal of Lightwave Technology*, vol. 34, no. 15, pp. 3646–3652, Aug. 2016.
[55] N. Andriolli, F. Fresi, F. Bontempi *et al.*, "InP monolithically integrated coherent transmitter," *Optics Express*, vol. 23, no. 8, p. 10741, Apr. 2015.
[56] K. Lawniczuk, C. Kazmierski, M. Wale *et al.*, "AWG-DBR-based WDM transmitter fabricated in an InP generic foundry platform," in *Optical Fiber Communications Conference and Exhibition (OFC), 2014*, Mar. 2014, p. Tu3H.2.
[57] S. Lange, R. Kaiser, M. Gruner *et al.*, "Low switching voltage InP-based travelling wave electrode Mach-Zehnder modulator monolithically integrated with DFB-laser for 60 Gb/s NRZ," in *Optical Fiber Communications Conference and Exhibition (OFC), 2015*, Mar. 2015, p. Th4E.1.
[58] Y. Sasahata, T. Saito, T. Takiguchi *et al.*, "Tunable DFB Laser Array Integrated With Mach-Zehnder Modulators for 44.6 Gb/s DQPSK Transmitter," *IEEE Journal of Selected Topics in Quantum Electronics*, vol. 19, no. 4, pp. 1 501 507–1 501 507, Jul. 2013.
[59] S. Kanazawa, T. Fujisawa, K. Takahata *et al.*, "Flip-Chip Interconnection Technique for Beyond 100-Gb/s (4 x 25.8-Gb/s) EADFB Laser Array Transmitter," *Journal of Lightwave Technology*, vol. 34, no. 2, pp. 296–302, Jan. 2016.
[60] S. Menezo, E. Temporiti, J. Lee *et al.*, "Transmitter Made up of a Silicon Photonic IC and its Flip-Chipped CMOS IC Driver Targeting Implementation in FDMA-PON," *Journal of Lightwave Technology*, vol. 34, no. 10, pp. 2391–2397, May 2016.
[61] M. J. Wale and C. Edge, "Self-aligned flip-chip assembly of protonic devices with electrical and optical connections," *IEEE Transactions on Components, Hybrids, and Manufacturing Technology*, vol. 13, no. 4, pp. 780–786, Dec. 1990.
[62] "Wafer scale Integration of Photonics and Electronics," http://cordis.europa.eu/project/rcn/199492_en.html, eU H2020 project.
[63] G. P. Agrawal and N. K. Dutta, *Semiconductor Lasers*. Boston, MA: Springer US, 1995, chapter 3, 6.

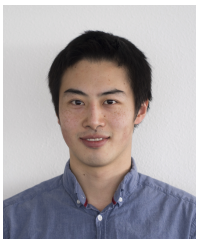

Weiming Yao received his B.Sc. degree in electrical engineering with honours from Technische Universität Berlin, Germany, in 2010, and graduated with two M.Sc. degrees in photonic networks engineering, with honours, as part of an Erasmus Mundus program from Aston University, Birmingham, UK, and Scuola Superiore Sant'Anna, Pisa, Italy, in 2012. Since then, he is with the Photonic Integration Group at Eindhoven University of Technology (TU/e) where his work focuses on the design and characterization of high bandwidth integrated multi-channel transmitter PICs. He received his Ph.D. from Eindhoven University of Technology with honours in 2017.

Meint K. Smit graduated in Electrical Engineering in 1974 at the Delft University of Technology in the Netherlands and received his Ph.D. in 1991, both with honours. He started research in Integrated Optics in 1981 and is inventor of the Arrayed Waveguide Grating, for which he received a LEOS Technical Achievement award in 1997 and the Rank Prize in 2016. He was closely involved in the introduction of MMI-couplers in semiconductor based Photonic IC technology. From 2000 to 2014 he was the chair of the Photonic Integration group at the COBRA Research Institute of Eindhoven University of Technology. His current research interests are in InP-based photonic integration, including integration of InP circuitry on Silicon. He is the founder of the JePPIX platform, the Joint European Platform for Photonic Integration of Components and Circuits, and strongly involved in the development of the InP-based photonic foundry system in Europe. Meint Smit is an IEEE Photonics Society Fellow and received an ERC Advanced Grant in 2012.

Michael J. Wale (M'92) received the B.A., M.A., and D.Phil. degrees in physics from the University of Oxford, U.K. He is the Director of Active Products Research at Oclaro Technology Ltd., based at Caswell, U.K. Since moving into industry in the early 1980s, he has been involved in many different aspects of research, development, and manufacturing of photonic devices and systems, with particular emphasis on photonic integrated circuit technology. Alongside his role at Oclaro, where he has responsibility for strategic technology activities, he is Professor of Photonic Integration/Industrial Aspects at Eindhoven University of Technology, The Netherlands, and an Honorary Professor at the University of Nottingham, U.K. He is a member of the Executive Board of the European Technology Platform, Photonics21, and the Chairman of its Working Group on Design and Manufacturing of Optical Components and Systems. He is a member of the Optical Society of America and is the author/co-author of approximately 200 publications.